

Clustering-Learning Approach to the Localization of Leaks in Water Distribution Networks

Luis Romero¹, Joaquim Blesa², Vicenç Puig³, and Gabriela Cembrano⁴

¹Institut de Robòtica i Informàtica Industrial (CSIC-UPC). Carrer Llorens Artigas, 4-6, 08028 Barcelona, Spain. Email: luis.romero.ben@upc.edu (corresponding author)

²Dr.Eng. Institut de Robòtica i Informàtica Industrial (CSIC-UPC). Carrer Llorens Artigas, 4-6, 08028 Barcelona, Spain; Supervision, Safety and Automatic Control Research Center (CS2AC) of the Universitat Politècnica de Catalunya, Campus de Terrassa, Gaia Building, Rambla Sant Nebridi, 22, 08222 Terrassa, Barcelona, Spain. Email: joaquim.blesa@upc.edu

³Dr.Eng. Institut de Robòtica i Informàtica Industrial (CSIC-UPC). Carrer Llorens Artigas, 4-6, 08028 Barcelona, Spain; Supervision, Safety and Automatic Control Research Center (CS2AC) of the Universitat Politècnica de Catalunya, Campus de Terrassa, Gaia Building, Rambla Sant Nebridi, 22, 08222 Terrassa, Barcelona, Spain. Email: vicenc.puig@upc.edu

⁴Dr.Eng. Institut de Robòtica i Informàtica Industrial (CSIC-UPC). Carrer Llorens Artigas, 4-6, 08028 Barcelona, Spain. Email: gabriela.cembrano@upc.edu

ABSTRACT

Leak detection and localization in water distribution networks (WDNs) is of great significance for water utilities. This paper proposes a leak localization method that requires hydraulic measurements and structural information of the network. It is composed by an image encoding procedure and a recursive clustering/learning approach. Image encoding is carried out using Gramian Angular Field (GAF) on pressure measurements to obtain images for the learning phase (for all possible leak scenarios). The recursive clustering/learning approach divides the considered region of the network into two sets of nodes using Graph Agglomerative Clustering (GAC), and trains a deep

neural network (DNN) to discern the location of each leak between the two possible clusters, using each one of them as inputs to future iterations of the process. The achieved set of DNNs is hierarchically organized to generate a classification tree. Actual measurements from a leak event occurred in a real network are used to assess the approach, comparing its performance with another state-of-the-art technique, and demonstrating the capability of the method to regulate the area of localization depending on the depth of the route through the tree.

INTRODUCTION

Nowadays water distribution networks (WDNs) are critical infrastructures in cities. Their efficient operation can reduce water losses, which are estimated to account for a 30% of the total amount of distributed water (Puust et al. 2010), producing high associated operational costs, as well as environmental (Xu et al. 2014) and sanitary (LeChevallier et al. 2003) problems. Thus, leak detection and localization approaches are widely researched (see (Chan et al. 2018) for an extensive review). The different solutions can be classified considering several aspects. One of the most important classifications separates model-based approaches from data-driven methodologies.

Model-based techniques rely on the estimation of hydraulic dynamics using mathematical models (Savić et al. 2009). A leak localization approach using pressure sensors, proposed in Pérez et al. (2014), compares pressure disturbances caused by a leak with a fault signature matrix obtained by means of hydraulic model simulations. This sensitivity analysis is also exploited in Sophocleous et al. (2019), included into a two-phase approach that uses search-space reduction to decrease the number of decision variables and their range of values, and an optimization strategy that solves the detection and localization problem. Another solution, presented in Sanz et al. (2015), compares calibrated parameters with historical values to find changes produced by a leak.

However, while model-based methods can work effectively under ideal conditions, their performance is limited by the availability and accuracy of the mathematical models (Menapace et al. 2018). Hydraulic models may contain structural modelling errors, nodal demand uncertainties and measurements noise (Blesa and Pérez 2018). Besides, the high computational cost and the uncertainty in parameter estimation hinder the application of these approaches. These drawbacks are

51 gradually overcome by the appearance of machine learning and data-driven procedures, which are
52 based on the mining of knowledge from the available data, gathered by installed sensor networks.

53 These methods typically use pressure sensors due to their lower cost in comparison to other
54 metering devices. In [Han et al. \(2018\)](#), a two-phase strategy is used to estimate the complete
55 state of the WDN from hydraulic heads at certain nodes by means of a Gauss-Newton Belief
56 Propagation inference scheme and to decompose the network to locate the leak. A deep-learning
57 (DL) framework is proposed in [Zhou et al. \(2019\)](#) to locate bursts using data from pressure sensors.
58 More recently, [Soldevila et al. \(2020\)](#) proposed a leak localization method that interpolates the
59 pressure at every node of the network from the measured values, comparing leak and leak-free
60 scenarios to locate the leak and using Dempster-Shafer reasoning to deal with uncertainty.

61 Other methodologies deal with additional types of sensors, mostly flow meters. A data-driven
62 method, proposed in [Arifin et al. \(2018\)](#), applies the concept of Kantorovich distance to detect
63 and locate leaks from flow rates and pressure measurements. In [Navarro et al. \(2019\)](#), a real time
64 leak localization method using Time Delay Neural Networks and flow/pressure measurements is
65 presented. A combined artificial neural network method is presented in [Pérez-Pérez et al. \(2021\)](#)
66 to perform leak diagnosis in pipes considering pressure and flow data.

67 Finally, other works deal with less common types of sensors. In [Kang et al. \(2017\)](#), data from
68 accelerometers is used to feed a two-stage approach, based on a convolutional neural network
69 (CNN) - support vector machine (SVM) architecture that detect leaks and a graph method based on
70 virtual nodes for their location. Besides, [Huang et al. \(2020\)](#) presents an efficient multistage leak
71 localization method that uses valve operations (VOs) to divide the demand metering area (DMA)
72 into two regions and water balance analysis based on smart demand meters to locate the leaks.

73 This paper proposes a leak localization method based on the use of the network topology and
74 pressure data from some inner nodes. The pressure information is encoded in the form of images, in
75 order to exploit the power of classical image-classification DL techniques. In this way, the degree of
76 freedom in the implementation of the method is higher, regarding the available software languages
77 and platforms. The localization operation is performed by means of a recursive clustering/learning

78 procedure. The structural information of the WDN is used by the clustering process to split a
79 certain (sub)network into two clusters of disjoint nodes, generating a set of binary labels. The
80 hydraulic images, together with the produced labels, feed a training process which must produce
81 a deep neural network (DNN) that indicates which one of the two generated clusters contains the
82 leak. The recursivity affects the clustering stage, since these clusters are provided as inputs of the
83 explained process for subsequent iterations. When all the generated DNNs are organized depending
84 on the hierarchy of their (sub)network, a classification tree is produced.

85 In comparison with previous DL-related works like [Javadiha et al. \(2019\)](#), a smart application
86 of the image-encoding process allows to limit the size of the images to be fed to the DL algorithm,
87 thus reducing the computational cost. Moreover, Moreover, it is guaranteed that the set of possible
88 candidates for the leak location are connected, due to the clustering stage dividing the (sub)network
89 into connected components. This feature provides a secondary advantage: if a hydraulic simulator
90 is not available to obtain the necessary pressure data for the training phase (hence using the strategy
91 as a mixed model-based/data-driven approach), leak experiments can be performed over certain
92 points of the real network after defining a set of subnetworks that will be the targets of the DNN
93 classification tree.

94 Additionally, the hierarchical structure of this classification tree allows to tackle one of the
95 main problems of learning-based leak localization methods: the similar effect of neighbouring
96 leaks in the hydraulic behaviour of the WDN. When this similitude affects a group of nodes,
97 it may become even impossible to discern the origin of the leak among them. The proposed
98 recursive clustering/learning approach handles this behaviour by retrieving information about the
99 classification limitations (directly related to the leaks resemblance) from the training performance
100 results at each level of the classification tree. Thus, the hierarchically organized DNNs of the trained
101 tree are applied to new samples if and only if the training accuracy was high enough. In this way,
102 an ad hoc solution for the studied WDN would be obtained, as it is adaptable to its characteristics
103 and limitations from the leak localization point of view. This fact demonstrates the qualitative
104 improvement at the leak localization solution that the proposed method offers in comparison with

105 strategies that lack this flexibility and hence provide unreliable solutions if the sensors amount
106 and/or precision are not appropriate.

107 Furthermore, some of the implemented techniques are adapted from their original design to
108 efficiently and effectively tackle their specific tasks, hence implying novelty in their exploitation.

109 **METHODOLOGY**

110 The proposed approach requires considering a set of assumptions, that should be fulfilled in
111 order to proceed with the method application:

- 112 • Pressure sensors are installed in a set of inner nodes. Besides, topological information about
113 the network must be available, i.e., the junctions connectivity and the pipes length.
- 114 • Records of pressure measurements are available for all possible leak cases. Since this
115 requirement may not be practical, these records could be obtained using a hydraulic simulator
116 and/or performing artificial leak experiments over a set of locations of the network. However,
117 this records are only needed at the off-line training stage.
- 118 • Due to the previous requirement, only single-leak scenarios are considered. The analysis
119 of multi-leak episodes would require data about every combination of leaks. Besides, the
120 leaks are supposed to appear at the network nodes, as usually considered in the literature
121 (Blesa and Pérez 2018; Sophocleous et al. 2019).
- 122 • The leak detection process is handled by an external method so that the proposed localization
123 technique is applied after a detection event occurs. A typical approach to detect the presence
124 of leaks consists of tracking changes in the night consumptions (Puust et al. 2010).

125 The following subsections describe the details of the methodology components and then the
126 general procedure thereof.

127 **Hydraulic Data Encoding**

128 The installation of pressure sensors allows to collect hydraulic information of the network state.
129 These measurements are converted into hydraulic heads by adding the elevation of each junction,

130 as these values are important to determine the availability of water service. The hydraulic heads
 131 are stored into data vectors (with a component for each sensor) that can be gathered at each time
 132 interval, considering the sampling time of the measuring devices.

133 Besides, as mentioned above, information about the widest possible range of leak scenarios is
 134 required, either from a hydraulic simulator or from artificial leak experiments at the real network.
 135 Concretely, considering the importance of the size of a leak in its effect on the WDN behaviour,
 136 the strategy that must be followed to handle different leak sizes must be adapted to the hydraulic
 137 information source:

- 138 • On the one hand, if a hydraulic simulator is available, different leak scenarios can be
 139 derived considering an estimated leak rate value, which can be obtained from an external
 140 leak detection method, as most of these approaches handle the estimation of the leak size.
- 141 • On the other hand, proper artificial leak experiments could be performed over the real WDN,
 142 considering that water utilities are usually interested in a concrete range of leak sizes that
 143 depends on the operational characteristics of their network.

144 The achieved hydraulic measurements can be arranged in a multidimensional matrix \mathbf{H} that
 145 stores the gathered data vectors: the value h_{ij}^l would represent the hydraulic head at time instant
 146 i of sensor j at leak scenario l , i.e., the leak is located at node l . The total number of time steps,
 147 sensors and possible leak scenarios will be referred to as M , N and P respectively. To highlight
 148 the time dependency, the notation h_{ij}^l is henceforth substituted by $h_j^l(i)$. Thus, a single data vector
 149 from the multidimensional matrix \mathbf{H} can be referred to as:

$$150 \quad \mathbf{h}^l(i) = [h_1^l(i), h_2^l(i), \dots, h_j^l(i), \dots, h_N^l(i)] \quad (1)$$

151 where each vector $\mathbf{h}^l(i)$ corresponds to a collection of the hydraulic heads of the N sensors for time
 152 instant i and leak scenario l .

153 The purpose of the data encoding process consists of converting the dataset \mathbf{H} composed by
 154 $M \cdot P$ vectors $\mathbf{h}^l(i) \in \mathbb{R}^N$ into a image set \mathbf{L} comprised by $M \cdot P$ images $L^l(i) \in \mathbb{R}^{N \times N}$.

155 The application of this process, despite the increase in the required memory space due to the
156 use of images, is justified by two main advantages:

- 157 1. In this way, the training stage can be tackled by means of standard DL techniques for image
158 classification, and hence a wide variety of tools are available for this task.
- 159 2. This procedure is handled by the Gramian Angular Field (GAF) method, presented in
160 [Wang and Oates \(2015\)](#) (concretely, the Gramian Summation Angular Field approach is
161 considered). It not only converts vectors into images, but also extracts correlations among
162 the components of the vector, enhancing the information provided to the learning stage.

163 However, the GAF technique has been adjusted to fulfil the requirements of a leak localization
164 approach: the novelty of its application lies in the selection of the vectors that are converted into
165 images. Despite its original design for the imaging of time-series, for this work, GAF is applied to
166 the hydraulic data vectors $\mathbf{h}^l(i)$. This is justified by the following key points:

- 167 • A small number of measuring devices is available at most of the WDNs ([Savić et al.](#)
168 [2009](#)). The reduced length N of the hydraulic information vectors $\mathbf{h}^l(i)$ implies a low
169 dimensionality of the generated images, greatly diminishing the computational cost of the
170 learning phase. Thus, the major drawback of the original usage of GAF is removed and the
171 application of post-processing techniques to reduce the image size is not required.
- 172 • The proposed selection of data vectors $\mathbf{h}^l(i)$ entails the training of the different DNNs with
173 a wide variety of time instants, hence generalizing the neural network learning by inducing
174 an independence of dynamical variables like the nodal demands.
- 175 • Besides, considering the opposite situation, the selection of time-series as the data vectors
176 for the imaging process (that is, the vectors \mathbf{h}_j^l of \mathbf{H}), would imply some drawbacks:
 - 177 1. The selection of a suitable time window $T < M$ (to split the complete time-series
178 into a set of time slots) would require analysing the length of the smallest set of time
179 instants whose information is rich enough to explain the leak location.

180 2. The collection of T -dimensional time-series would be required to feed the leak
 181 localization algorithm. This implies the existence of a minimum necessary time
 182 lapse to achieve a single localization.

183 GAF exploits the angular perspective of the polar-encoded hydraulic information. Thus, each
 184 input vector is rescaled to a range of values between -1 and 1 to fit the image of the cosine function.
 185 The vector $\mathbf{h}^l(i)$ is processed as follows:

$$\tilde{h}_j^l(i) = \frac{2h_j^l(i) - (\max(\mathbf{h}^l(i)) + \min(\mathbf{h}^l(i)))}{\max(\mathbf{h}^l(i)) - \min(\mathbf{h}^l(i))} \quad (2)$$

$$\phi_j^l(i) = \arccos(\tilde{h}_j^l(i)) \quad (3)$$

186 By considering the trigonometric sum between each pair of polar-encoded head values, the
 187 associated GAF image is generated:

$$L^l(i) = [\cos(\phi_a^l(i) + \phi_b^l(i))] = (\tilde{\mathbf{h}}^l(i))' \cdot \tilde{\mathbf{h}}^l(i) - \left(\sqrt{\mathbf{1}_N - (\tilde{\mathbf{h}}^l(i))^2}\right)' \cdot \sqrt{\mathbf{1}_N - (\tilde{\mathbf{h}}^l(i))^2} \quad (4)$$

188 where a and b are possible values of j and $\mathbf{1}_N$ is the unit row vector of length N .

189 The resulting image $L^l(i)$ is a $N \times N$ matrix whose $a - b$ component encodes the relation
 190 between the heads at the sensorized nodes a and b . Each $L^l(i)$ is processed to scale its values in
 191 the range 0-255 to use the standard format of an image, achieving the rescaled dataset $\bar{\mathbf{L}}$.

192 **Recursive Clustering/Learning**

193 Once the image set $\bar{\mathbf{L}}$ has been generated, the recursive clustering/learning stage uses this
 194 information, as well as the WDN topology, to produce the previously mentioned classification tree.

Clustering stage

In order to manage the topology of a network, let us model its structure by means of a graph represented as $\mathcal{G} = (\mathcal{V}, \mathcal{E})$. \mathcal{V} stands for the set of nodes/junctions and \mathcal{E} is the set of edges/pipes. A node is represented as $v_x \in \mathcal{V}$ while $e_{xy} = (v_x, v_y) \in \mathcal{E}$ denotes an edge connecting v_x and v_y . Nodes from \mathcal{V} are said to be adjacent if they are connected by edges in \mathcal{E} . Each edge e_{xy} is associated to a weight w_{xy} , and hence a weighted adjacency matrix $W \in \mathbb{R}^{N \times N}$ can be constructed:

$$w_{ij} = \begin{cases} c_{ij}, & \text{if } e_{ij} \in \mathcal{E} \\ 0, & \text{otherwise} \end{cases} \quad (5)$$

where c_{ij} represents the length of the pipe connecting junctions v_i and v_j .

An extended version of W that stores the relation among all the nodes in the network can be derived: a non-adjacent pair of nodes, i.e., $e_{xy} = (v_x, v_y) \notin \mathcal{E}$, is given an estimated weight \hat{w}_{xy} , computed as the sum of the weights of the edges composing the shortest path (see Festa (2006) for an extensive review about algorithms for its computation) from v_x to v_y , and this translates to the sum of the lengths of the pipes in this shortest path. Thus, it can be regarded as a pairwise distance matrix, referred to as $\hat{W} \in \mathbb{R}^{N \times N}$.

The structural information stored in \hat{W} is exploited by the Graph Agglomerative Clustering (GAC) method, developed in Zhang et al. (2013) to segment the nodes of a graph into clusters. Basically, the GAC approach performs an operation composed of three main phases:

1. A k -nearest-neighbours (k -NN) graph (see the introduction in Wang et al. (2012) for a formal definition) is generated from the provided pairwise distance matrix \hat{W} by means of the computation of an asymmetric weighted adjacency matrix.
2. A set of small clusters is computed considering the *weakly connected components* (Pemmaraju and Skiena 2003) of the k -NN graph with a low neighbourhood size k .
3. Those clusters are iteratively merged into larger ones until the settled number of clusters is reached, selecting the two clusters with the highest affinity at each iteration.

219 In this work, *graph average linkage* (Sokal and Michener 1958) is chosen as the agglomerative
 220 clustering algorithm that handles the affinity comparison. It uses the edge weights of the k -NN
 221 graph as the similarity metric, averaging the values between clusters.

222 Once the clustering procedure is performed, two disjoint sets of nodes are obtained, i.e., $\mathcal{L}_1 \subseteq \mathcal{V}$
 223 and $\mathcal{L}_2 \subseteq \mathcal{V}$ holding that $\mathcal{L}_1 \cap \mathcal{L}_2 = \emptyset$ and $\mathcal{L}_1 \cup \mathcal{L}_2 = \mathcal{V}$. Assigning a different label to each
 224 subset, a label or target vector $\mathbf{t} \in \mathbb{R}^N$ can be derived:

$$225 \quad t_x = \begin{cases} 1, & \text{if } v_x \in \mathcal{L}_1 \\ 2, & \text{if } v_x \in \mathcal{L}_2 \end{cases} \quad \forall x = 1, \dots, N \quad (6)$$

226 The GAC process, as explained for graph $\mathcal{G} = (\mathcal{V}, \mathcal{E})$ (corresponding to the complete WDN),
 227 is also applicable to graph $\mathcal{G}_{\mathcal{L}} = (\mathcal{L}, \mathcal{E}_{\mathcal{L}})$ (associated to a certain subset of nodes \mathcal{L}), hence
 228 allowing the recursiveness of the clustering strategy. Similarly, the pairwise distance matrix and
 229 the targets vector would be $\hat{W}_{\mathcal{L}} \in \mathbb{R}^{|\mathcal{L}| \times |\mathcal{L}|}$ and $\mathbf{t}_{\mathcal{L}} \in \mathbb{R}^{|\mathcal{L}|}$ respectively.

230 Several aspects about the implementation of the clustering strategy must highlighted due to
 231 their importance with regard to the requirements of the leak localization method:

- 232 • Each clustering operation produces two clusters due to the binary classification approach.
- 233 • The pairwise distance matrix \hat{W} associates a higher cost to distance nodes than to close
 234 nodes.
- 235 • The value of parameter k directly influences the generation of the required k -NN graph by
 236 setting the size of the considered neighbourhoods. For each clustering operation, depending
 237 on the cardinality $|\mathcal{L}|$ of the node set of graph $\mathcal{G}_{\mathcal{L}}$, it is computed as follows:

$$238 \quad k_{\mathcal{L}} = \text{randi}(|\mathcal{L}| - o) + o - 1 \quad (7)$$

239 where $\text{randi}(X)$ is a function generating a pseudo random integer from 1 to X , and o is an
 240 offset, which must be set for the studied network, in order to discard possible values that
 241 are too close to 1 and X .

Learning stage

The above-described procedure provides the last ingredient for the learning phase. On the one hand, the complete dataset of images $\bar{\mathbf{L}}$, composed of $M \cdot P \cdot N \times N$ samples, is obtained from the image encoding process. However, only $M \cdot |\mathcal{X}|$ images would be applicable if considering an arbitrary iteration of the recursive clustering/learning approach that operates over $\mathcal{G}_{\mathcal{X}}$. Furthermore, considering that only M_{tr} time instants out of the M available ones are used for training purposes, the final number of training images corresponds to $M_{tr} \cdot |\mathcal{X}|$.

On the other hand, a vector of labels $\mathbf{t}_{\mathcal{X}}$ was obtained from the clustering strategy. It must be repeated M_{tr} times to produce $\mathbf{t}_{\mathcal{X}}^{ext} \in \mathbb{R}^{M_{tr} \cdot |\mathcal{X}|}$, which matches the length of the samples set.

Apart from the described training target set, the validation and testing sets must be generated. Whereas the training set is employed during the learning phase to update the DNN parameters, the validation set is used periodically in the same phase to assess the DNN accuracy. Finally, the testing set is employed to evaluate the final performance of the DNN, once trained. Their lengths would be $M_{val} \cdot |\mathcal{X}|$ and $M_{test} \cdot |\mathcal{X}|$ respectively, with $M_{val}, M_{test} < M$. These sets are used to train, validate and test DNNs as shown in Fig. 1.

The procedure is designed to be complete enough to extract features from the images and to use them to learn how to classify those images, as well as simple enough to reduce the computational cost of the training process. Additionally, the design is conceived to be general enough to be applicable to different networks, as the only configuration parameter that is related to the studied WDN is the number of sensors. The DL structure is composed by a set of three layers, associated to different roles during the learning process, namely:

1. Convolutional layer (C in Fig. 1): It applies sliding convolutional filters to its input, extracting key features that allow to assign a label to the analysed image (Murphy 2016).
2. Batch normalization layer (BN in Fig. 1): It normalizes its inputs (outputs of the convolutional layer) over each input channel (there is one channel per filter in the associated convolution) and over a concrete mini-batch, i.e., the set of samples processed before updating the model parameters. This technique speeds up the training and reduces the dependence

269 on the initialization of the DNN. Besides, it adds a regularization effect due to the partition
270 of the dataset in mini-batches and the associated parameter update only occurring after a
271 complete mini-batch is analysed (Ioffe and Szegedy 2015).

- 272 3. ReLu layer: The ReLu layer applies a non-linear activation function to its inputs. It consists
273 of a threshold operation, setting to zero any negative value (Agarap 2018).

274 After the instances of the presented set of layers, a fully connected network (FCN) is applied.
275 It multiplies its input by a weight matrix and adds a bias vector, combining the features learned
276 by the previous layers to identify larger patterns. Finally, a *softmax* layer (Bishop 2006) is used to
277 compute the conditional probability of each one of the classes for the analysed sample.

278 Procedure Overview

279 The above-described elements and processes pursue the goal of the generation and subsequent
280 application of a classification tree, formed by the hierarchical organization of the trained DNNs.

281 *Classification tree generation*

282 The generation of the classification tree is an off-line operation, carried out with pre-collected
283 measurements and the available network topology, as summarised in Fig. 2.

284 The algorithm starts with a preprocessing stage, where the graph associated to the WDN
285 structure is extracted, and the hydraulic measurements at the available historical dataset of leaks
286 are converted into an image set, by means of the described image encoding process.

287 Then, the recursive clustering/learning operation is executed until the number of iterations
288 reaches a certain limit. Each iteration is repeated until the testing accuracy of the considered
289 DNN reaches a predefined threshold. Re-training may be performed to check the suitability of
290 the k parameter of the clustering algorithm, which is initially random to explore the range of
291 possible values while pursuing an effective performance of the DNN. For every generated k , the
292 corresponding (sub)network is clustered and the labels are obtained. Taking into account that the
293 image samples are already available and divided into learning (including training and validation)
294 and testing sets, the learning process is performed. If the testing accuracy is good enough, the

295 current iteration will be finalized by adding the subnetworks generated during the clustering at the
296 bottom of a queue that stores the subnetworks to be clustered in subsequent iterations.

297 Once the process is finished, all the trained DNNs are organized depending on their correspond-
298 ing (sub)network, obtaining the classification tree: the result of the application of a certain DNN
299 of the tree indicates the next DNN to be used, continuously functioning in this way from the first
300 DNN, which operates over the complete WDN, to the desired depth.

301 The classification tree generation scheme has an additional advantage: the testing accuracy at
302 the different levels of depth of the tree allows to gain crucial knowledge about the limitations of the
303 leak localization process, regarding issues like the WDN structure and the sensorization properties,
304 i.e., the amount, distribution and precision of the sensors. All the gathered information about these
305 limitations allows the operator to decide a proper depth for the application of the tree.

306 *Classification tree application*

307 This procedure is represented by the flow chart of Fig. 3.

308 The application of the classification tree is carried out online, and hence hydraulic measurements
309 are converted into an image that is provided to the trained classification tree in real-time, in order to
310 locate an occurring leak once it has been detected. The depth to traverse through the tree is decided
311 considering the gained knowledge about the limitations of the leak localization process.

312 Firstly, the top DNN of the tree is fed with the generated image, obtaining a label which indicates
313 the subnetwork where the leak is located from the two possible clusters. This label indicates the
314 next DNN to apply, and the process is repeated until the localization depth is reached. Then, the
315 application of the final DNN provides the set of candidates where the leak can be located.

316 **CASE STUDY**

317 The application of the presented methodology is illustrated by means of a case study. It corre-
318 sponds to a District Metering Area (DMA) (see [Savić and Ferrari \(2014\)](#) for extensive information
319 about DMAs) from a real network referred to as E-Town. It is graphically represented in Fig. 4.

320 The considered DMA is formed by 125 pipes and 120 inner nodes, of which 8 are equipped
321 with pressure sensors (pink stars at Fig. 4). The water supplied to the area is obtained from a single

322 water inlet (green square at Fig. 4.). The location of a real leak, that will be studied to show the
323 methodology performance, is indicated with a red hexagram at Fig. 4.

324 **Hydraulic Data Encoding For E-Town**

325 In order to illustrate the image encoding process, Fig. 5 and Fig. 6 respectively show the GAF
326 images associated to eight nodes of E-Town and their locations, at a certain time instant.

327 As mentioned above, the approach requires hydraulic information of the complete range of
328 possible leaks. In this work, EPANET 2 (Rossman 2000) is used to simulate the necessary leak
329 scenarios. Since only eight sensors are installed, the associated images have a size of 8×8 . A pixel
330 ij of the image encodes the relation between components i and j of the data vector.

331 The majority of the GAF images presented in Fig. 5 exhibit clear differences among them due
332 to the effect of the leaks on the readings of the different sensors. These differences are exploited
333 by the DL algorithm to discern the leak location between the possible clusters. However, in the
334 case of nodes 39 (Fig. 5c) and 58 (Fig. 5f), which correspond to rather close junctions, little
335 differences appear between their images. Both facts illustrate the suitability of an approach that
336 allows to regulate the localization area: the location at node-level is nearly impossible, due to the
337 extremely slight differences of the corresponding leak effects. Hence, a trade-off between location
338 accuracy and area must be considered while applying the classification tree in order to optimize the
339 methodology performance.

340 **Recursive Clustering/Learning For E-Town**

341 The iterative application of the clustering process up to a third level of depth is shown at Fig. 7.

342 The produced clusters clearly arise from a topological perspective, partitioning the (sub)networks
343 at links that connect distant nodes. However, it is interesting to remark the specific case of sub-
344 networks 1.1 and 1.2.1 (referring to the numbering in Fig. 7, which are split into two sets that are
345 very different in size. This effect is produced by the explained re-training policy, which repeats
346 the learning stage of the corresponding iteration, modifying the k parameter of the clustering, in
347 search for a testing accuracy that reaches the desired threshold (a 95% in the cases at Fig. 7.
348 Thus, the clustering depends on the network structure, but it is also indirectly affected by the leak

349 information, since the learning phase also seeks to improve the localization.

350 For the learning stage, the DL architecture has been implemented using the MATLAB® Deep-
351 Learning Toolbox™. The learning process is configured by means of the following parameters:

- 352 • Solver: It specifies the algorithm to be used. Stochastic Gradient Descent with Momentum
353 (Qian 1999) is selected, keeping the default momentum value of 0.9. In this way, the
354 oscillations along the path of the steepest descent towards the optimal point are reduced.
- 355 • Learning rate: It is configured by means of four parameters, whose values are tuned and
356 refined to maximize the classification accuracy:
 - 357 • Initial learning rate: It is the value at the start of the training and it is set to 0.01.
 - 358 • Learning rate schedule: It is set to decrease the learning rate piecewise during the
359 training, after a certain number of epochs, by multiplying it by a factor. This is
360 interesting to refine the learning process at the final steps.
 - 361 • Learning rate dropping period: It corresponds to the required number of epochs to
362 drop the learning rate. It is settled to 8 epochs, to maintain each learning rate value
363 a minimum number of iterations.
 - 364 • Learning rate dropping factor: It is the multiplicative factor that affects the learning
365 rate every learning rate dropping period and it is configured to 0.9.
- 366 • Convolutional filter size: It settles the length of the square filters at the convolutional layers.
367 These lengths are different for each one of the three instances of the set of layers presented
368 in the explanation of Fig. 1, and they depend on the number of sensors N to facilitate the
369 adaptation to different networks: $[\lfloor N/2 \rfloor \lfloor N/3 \rfloor \lfloor N/4 \rfloor]$.
- 370 • Number of filters: It corresponds to the number of filters at each one of the convolutional
371 layers: [8, 16, 32].

372 The rest of available parameters are maintained as default. The image/label set is shuffled
373 before every epoch in order to improve the regularizing effect of the batch normalization, as the

374 activation of a concrete image during training depends on the rest of images of the mini-batch. The
375 division of the dataset at each learning operation includes a 75% for training, a 15% for validation
376 and a 10% for testing purposes. The different neural networks composing the classification tree are
377 trained by means of a NVIDIA GeForce MX130 GPU and a Intel® Core™ i7-8565U processor.

378 RESULTS

379 A real leak event was evaluated with the trained classification tree to evaluate the goodness of
380 the solution. The leak is estimated to have a size of 1.15 l/s, and hence the DNNs were trained with
381 hydraulic data obtained using EPANET2 and considering this leak size. The dataset of the real leak
382 pressure measurements is composed of 720 entries (that is, 24 hours with a sampling period of 2
383 minutes) which are affected by different sources of uncertainty due to their real nature. Therefore,
384 the EPANET2 scenarios were generated considering a 5% of uncertainty at the user water demands
385 and the pipe roughnesses. Moreover, in order to consider the measurement noise in the sensors,
386 the data from the hydraulic simulator was truncated to emulate a sensor precision of ± 0.01 m. The
387 location of the leak in E-Town is indicated in Fig. 4.

388 The application of the classification tree to the real leak data is graphically presented in Fig.
389 8. The green line circles indicates the subnetwork that is selected by the localization algorithm at
390 each level of the tree. The black cross marks the location of the real leak.

391 The information from the figure can be completed by these numeric results:

- 392 • Considering the levels from (a) to (c) (the letters refer to the coding at Fig. 8), the localization
393 is properly performed, as the leaky node is located in the highlighted area. This area is
394 composed by a total of 34 nodes, with a mean pipe distance of 576.41 m from these nodes
395 to the leaky one. Moreover, 8 clusters are formed at this level of depth of the tree, i.e., 8
396 possible outcomes of the algorithm if the tree is traversed until this depth.
- 397 • At level (d), the localization remains correct, reducing the localization region to 16 nodes
398 and the mean pipe distance to 357.02 m. There are 16 final clusters at this level of depth.
- 399 • Progressing to level (e), the correct localization diminishes the number of nodes to 13 and

400 the mean pipe distance to 335.18 m while the number of final clusters adds up to 29.

- 401 • However, at level (*f*), the localization turns out to be incorrect, as the leaky node is not
402 considered in the localization area, which is formed by 11 nodes. The mean pipe distance
403 and the number of final clusters get increased to 393.62 m and 52 respectively.
- 404 • Considering levels from (*g*) to (*h*), the incorrect localization continues increasing both the
405 mean pipe distance and the number of final clusters to 418.98 m and 85 respectively, whereas
406 6 nodes are included at the achieved localization region.
- 407 • Finally, considering the single-node level (which implies the existence of 120 clusters, one
408 per node), the pipe distance from the reached node to the leaky one is 442.01 m.

409 DISCUSSION

410 Several aspects can be discussed about the presented results:

- 411 • The localization operation works properly until the (*f*)-level is reached, referring both Fig.
412 8 and presented numerical results. Therefore, branch (*e*) of the tree would correspond to
413 the localization area limit regarding the region where the real leak is located.
- 414 • The mean pipe distance is increased by the amount of nodes at early stages of the tree,
415 as well as the large separation between nodes of interest. For example, the pipe distance
416 between the leaky node and its neighbour from the right is 267.25 m.
- 417 • Regarding the final number of nodes at level (*e*), the search area is successfully reduced to
418 approximately a 10% of the total network. The value of 29 final clusters at this level shows
419 that the clusters of the region of the leak are quite big in comparison with the rest of the
420 network. The heterogeneity of the density of nodes per cluster at the different regions is
421 produced by the network structure and the re-training approach.

422 The performance of the proposed localization approach for the considered real leak can be
423 compared with that of a well-known model-based methodology, based on a fault sensitivity analysis
424 of the residuals (Casillas et al. 2013). The application of this strategy is represented in Fig. 9.

425 The light blue nodes of this figure and the red ones at level (*e*) of Fig. 8 correspond to a similar

426 region of the network, and therefore the localization result of the proposed methodology can match
427 the degree of performance of a model-based state-of-the-art technique. Furthermore, the proposed
428 method produces an even more accurate result:

- 429 • Regarding the exact localization, the model-based strategy indicates a node that is 501 m
430 away from the real leak, while the proposed approach finds a node that is 442 m away.
- 431 • About the selected area of localization, the proposed methodology produces a more precise
432 result due to the exclusion of outliers, whereas the model-based method highlights one.

433 Therefore, the aforementioned model-based method is outperformed at both the leak candidate
434 set selection and the node-level localization by the proposed methodology. Regarding these two
435 aspects, it is important to focus on the selected area of localization because it is directly related
436 to one of the novelties of the proposed approach in comparison with previous methods: the
437 hierarchical organization of the classification tree. The differences between training data (which
438 in this case is obtained from a simulator) and real measurements may introduce errors at the node-
439 level localization, but the classification tree can be traversed backwards in order to search the leak
440 at a larger set of nodes, which are also guaranteed to be in the same area of the network due to
441 the topology-based clustering. This characteristic entails an advantage in comparison with other
442 methodologies: for example, in the case of the compared model-based approach, there exists an
443 outlier in the final set of most probable leak origins (the light blue point in Fig. 9 that is located out
444 of the branch where the leak occurs) that hinders the localization of the real location of the leak.

445 **CONCLUSIONS**

446 This article presents a leak localization approach based on image encoding, graph-based clus-
447 tering and deep-learning. It uses information about the different possible leak events at a WDN,
448 converted into images via a data encoding process, to produce a classification tree by means of a
449 recursive clustering/learning approach. The techniques selected to perform these operations are
450 configured and applied in customized ways to fit the necessities of the leak localization task.

451 The application of the methodology allows to naturally gain knowledge about the leak local-

452 ization limitations due to the sensors accuracy, placement and number, as well as network charac-
453 teristics. Accordingly, the best leak localization area can be selected, as the classification tree can
454 be traversed from the first clustering of the complete network to any pre-trained intermediate state
455 until the single-node level is reached. Besides, this localization-area-based approach guarantees the
456 selection of congregated nodes due to the exploitation of the structural and topological information.

457 The method has been applied to the case of a leak at a real network, using data from the actual
458 WDN. The results are compared to the performance of another state-of-the-art technique, showing
459 improvements regarding both the leak localization area definition and the node-level operation.

460 Some tasks remain open regarding the research in this field. On the one hand, a review of the
461 different components of the methodology can be performed to find even more suitable elements to
462 substitute the current ones. On the other hand, regarding the selected methods, their configuration
463 and calibration can be improved by means of their inputs and parameters. Furthermore, extra studies
464 about the effect of uncertainty and inaccuracies at the hydraulic model, sensor measurements and
465 network characteristics can be performed in order to analyse the sensitivity of the method to those
466 aspects. Finally, it could be interesting to test the methodology considering that the hydraulic
467 model of the WDN is not available, that is, working together with a water utility to perform several
468 artificial leak experiments to gather data for the training of the DNNs.

469 **DATA AVAILABILITY STATEMENT**

470 All data, models, or code generated or used during the study are proprietary or confidential
471 in nature and may only be provided with restrictions. Specifically, there is a hard restriction in
472 the sharing of information about the studied network: features, location, the hydraulic information
473 from the real leak event, etc. The associated codes could be shared upon reasonable request.

474 **ACKNOWLEDGEMENTS**

475 The authors want to thank the Spanish national project DEOCS (DPI2016-76493-C3-3-R)
476 and the Spanish State Research Agency through the María de Maeztu Seal of Excellence to IRI
477 (MDM-2016-0656). Joaquim Blesa acknowledges the support from the Serra Húnter program.

REFERENCES

- Agarap, A. (2018). “Deep learning using rectified linear units (relu).” *Preprint arXiv:1803.08375*.
- Arifin, B., Li, Z., Shaha, S., Meyer, G., and Colin, A. (2018). “A novel data-driven leak detection and localization algorithm using the Kantorovich distance.” *Comput. Chem. Eng.*, 108, 300–313 <https://doi.org/10.1016/j.compchemeng.2017.09.022>.
- Bishop, C. (2006). “Probability distributions - The exponential family.” *Pattern Recognition and Machine Learning*, Springer, New York, NY.
- Blesa, J. and Pérez, R. (2018). “Modelling uncertainty for leak localization in water networks.” *IFAC-PapersOnLine*, 51(24), 730–735 <https://doi.org/10.1016/j.ifacol.2018.09.656>.
- Casillas, M., Garza-Castañón, L., and Puig, V. (2013). “Model-based leak detection and location in water distribution networks considering an extended-horizon analysis of pressure sensitivities.” *J. of Hydroinform.*, IWA, 16(3), 649–670 <https://doi.org/10.2166/hydro.2013.019>.
- Chan, T. K., Chin, C. S., and Zhong, X. (2018). “Review of current technologies and proposed intelligent methodologies for water distributed network leakage detection.” *IEEE Access*, 6, 78846–78867 <https://doi.org/10.1109/ACCESS.2018.2885444>.
- Festa, P. (2006). “Shortest path algorithms.” *Handbook of Optimization in Telecommunications*, M. Resende and P. Pardalos, eds., Springer, Boston, MA, 185–210.
- Han, Q., Eguchi, R., Mehrotra, S., and Venkatasubramanian, N. (2018). “Enabling state estimation for fault identification in water distribution systems under large disasters.” *IEEE 37th Symp. on Reliable Distributed Systems (SRDS)*, IEEE, Salvador, Bahia, Brazil, 161–170. <https://doi.org/10.1109/SRDS.2018.00027>.
- Huang, Y., Zheng, F., Kapelan, Z., Savić, D., Duan, H.-F., and Zhang, Q. (2020). “Efficient leak localization in water distribution systems using multistage optimal valve operations and smart demand metering.” *Water Resour. Res.*, 56(10), e2020WR028285 <https://doi.org/10.1029/2020WR028285>.
- Ioffe, S. and Szegedy, C. (2015). “Batch normalization: Accelerating deep network training by reducing internal covariate shift.” *ICML’15 Proceed. 32nd Inter. Conf. on M.L.*, Vol. 37, ICML.

505 Javadiha, M., Blesa, J., Soldevila, A., and Puig, V. (2019). “Leak localization
506 in water distribution networks using deep learning.” *2019 6th International Confer-
507 ence on Control, Decision and Information Technologies (CoDIT)*, IEEE, 1426–1431.
508 <https://doi.org/10.1109/CoDIT.2019.8820627>.

509 Kang, J., Park, Y.-J., Lee, J., Wang, S.-H., and Eom, D.-S. (2017). “Novel leakage detection by
510 ensemble cnn-svm and graph-based localization in water distribution systems.” *IEEE Trans. Ind.
511 Electron.*, 65(5), 4279–4289 <https://doi.org/10.1109/TIE.2017.2764861>.

512 LeChevallier, M. W., Gullick, R. W., Karim, M. R., Friedman, M., and Funk, J. E. (2003). “The
513 potential for health risks from intrusion of contaminants into the distribution system from pressure
514 transients.” *J. Water Health*, 1(1), 3–14 <https://doi.org/10.2166/wh.2003.0002>.

515 Menapace, A., Avesani, D., Righetti, M., Bellin, A., and Pisaturo, G. (2018). “Uni-
516 formly distributed demand EPANET extension.” *Water Resour. Manag.*, 32(6), 2165–2180
517 <https://doi.org/10.1007/s11269-018-1924-6>.

518 Murphy, J. (2016). “An overview of convolutional neural network architectures for deep learning.”
519 *Microway Inc*.

520 Navarro, A., Begovich, O., Delgado-Aguíñaga, J., and Sánchez, J. (2019). “Real time leak
521 isolation in pipelines based on a time delay neural network.” *2019 IEEE International Au-
522 tumn Meeting on Power, Electronics and Computing (ROPEC)*, IEEE, Ixtapa, Mexico, 1–6.
523 <https://doi.org/10.1109/ROPEC48299.2019.9057112>.

524 Pemmaraju, S. and Skiena, S. (2003). “Strong and Weak Connectivity - Connectivity - Properties
525 of Graphs.” *Computational Discrete Mathematics: Combinatorics and Graph Theory with
526 Mathematica®*, M. Resende and P. Pardalos, eds., Cambridge University Press.

527 Pérez, R., Sanz, G., Puig, V., Quevedo, J., Cugueró-Escofet, M. À., Nejjari, F., Meseguer, J.,
528 Cembrano, G., Mirats-Tur, J. M., and Sarrate, R. (2014). “Leak localization in water networks: a
529 model-based methodology using pressure sensors applied to a real network in Barcelona.” *IEEE
530 Control Syst.*, 34(4), 24–36 <https://doi.org/10.1109/MCS.2014.2320336>.

531 Pérez-Pérez, E., López-Estrada, F., Valencia-Palomo, G., Torres, L., Puig, V., and Mina-Antonio,

532 J. (2021). “Leak diagnosis in pipelines using a combined artificial neural network approach.”
533 *Control Eng. Practice*, 107, 104677 <https://doi.org/10.1016/j.conengprac.2020.104677>.

534 Puust, R., Kapelan, Z., Savić, D., and Koppel, T. (2010). “A review of meth-
535 ods for leakage management in pipe networks.” *Urban Water J.*, 7(1), 25–45
536 <https://doi.org/10.1080/15730621003610878>.

537 Qian, N. (1999). “On the momentum term in gradient descent learning algorithms.” *Neural Netw.*,
538 Elsevier, 12(11), 145–151 [https://doi.org/10.1016/S0893-6080\(98\)00116-6](https://doi.org/10.1016/S0893-6080(98)00116-6).

539 Rossman, L. A. (2000). *EPANET 2 User’s Manual*. Washington, D.C.

540 Sanz, G., Pérez, R., Kapelan, Z., and Savić, D. (2015). “Leak detection and localization through
541 demand components calibration.” *J. Water Resour. Plan. and Manag.*, ASCE, 142(2), 04015057
542 [https://doi.org/10.1061/\(ASCE\)WR.1943-5452.0000592](https://doi.org/10.1061/(ASCE)WR.1943-5452.0000592).

543 Savić, D. and Ferrari, G. (2014). “Design and performance of district metering areas in water distri-
544 bution systems.” *Procedia Eng.*, 89, 1136–1143 <https://doi.org/10.1016/j.proeng.2014.11.236>.

545 Savić, D. A., Kapelan, Z. S., and Jonkergouw, P. M. (2009). “Quo vadis water distribution model
546 calibration?.” *Urban Water J.*, 6(1), 3–22 <https://doi.org/10.1080/15730620802613380>.

547 Sokal, R. and Michener, C. (1958). “A statistical method for evaluating systematic relationships.”
548 *Univ. Kansas, Sci. Bull.*, 38, 1409–1438.

549 Soldevila, A., Blesa, J., Jensen, T. N., Tornil-Sin, S., Fernández-Cantí, R. M., and
550 Puig, V. (2020). “Leak localization method for water-distribution networks using a
551 data-driven model and Dempster-Shafer reasoning.” *IEEE Trans. Control Syst. Technol.*
552 <https://doi.org/10.1109/TCST.2020.2982349>.

553 Sophocleous, S., Savić, D., and Kapelan, Z. (2019). “Leak localization in a real water distribution
554 network based on search-space reduction.” *J. Water Resour. Plan. and Manag.*, ASCE, 145(7),
555 04019024 [https://doi.org/10.1061/\(ASCE\)WR.1943-5452.0001079](https://doi.org/10.1061/(ASCE)WR.1943-5452.0001079).

556 Wang, D., Zheng, Y., and Cao, J. (2012). “Parallel construction of approximate knn graph.”
557 *11th Inter. Symp. on Distrib. Comput. and App. to Business, Eng. & Sc.*, IEEE, 22–26.
558 <https://doi.org/10.1109/DCABES.2012.87>.

- 559 Wang, Z. and Oates, T. (2015). “Imaging time-series to improve classification and imputation.”
560 *24th Inter. Joint Conf. on Artif. Int.*, IJCAI, Buenos Aires, Argentina, 3939–3945.
- 561 Xu, Q., Liu, R., Chen, Q., and Li, R. (2014). “Review on water leakage control in distribu-
562 tion networks and the associated environmental benefits.” *J. Environ. Sci.*, 26(5), 955–961
563 [https://doi.org/10.1016/S1001-0742\(13\)60569-0](https://doi.org/10.1016/S1001-0742(13)60569-0).
- 564 Zhang, W., Zhao, D., and Wang, X. (2013). “Agglomerative clustering via
565 maximum incremental path integral.” *Pattern Recognit.*, 46(11), 3056–3065
566 <https://doi.org/10.1016/j.patcog.2013.04.013>.
- 567 Zhou, X., Tang, Z., Xu, W., Meng, F., Chu, X., Xin, K., and Fu, G. (2019). “Deep learning
568 identifies accurate burst locations in water distribution networks.” *Water Res.*, 166, 115058
569 <https://doi.org/10.1016/j.watres.2019.115058>.

570
571
572
573
574
575
576
577
578
579
580
581
582
583
584
585
586
587
588
589

List of Figures

1	Deep neural network structure.	25
2	Flow chart of the methodology steps for the learning (off-line) stage.	26
3	Flow chart of the methodology steps for the application (online) stage.	27
4	Schematic representation of E-Town.	28
5	A comparison among the GAF images associated to eight different leak events is presented. In appearing order: (a) Node 4, (b) Node 29, (c) Node 39, (d) Node 41, (e) Node 43, (f) Node 58, (g) Node 85 and (h) Node 94.	29
6	Location of the considered nodes for the GAF demonstration.	30
7	Clustering results for E-Town until 8 clusters are achieved.	31
8	Graphical summary of the localization process performance: (a) Complete network, (b) Subnetwork of the cluster selected from (a), (c) Subnetwork of the cluster selected form (b), (d) Subnetwork of the cluster selected form (c), (e) Subnetwork of the cluster selected form (d), (f) Subnetwork of the cluster selected form (e), (g) Subnetwork of the cluster selected form (f), (h) Subnetwork of the cluster selected form (g).	32
9	Result of the application of a model-based approach to the leak localization of the real leak. (a) Correlations map - the bluer the node, the higher the correlation, and hence, the higher the probability of the node to be the origin of the leak. (b) Zoom of the most probable leak area.	33

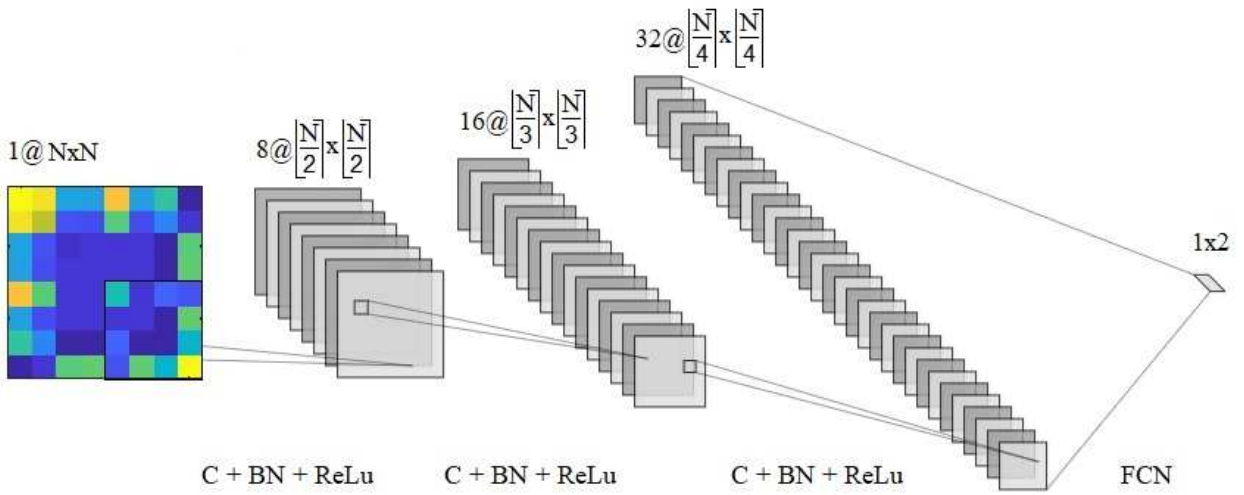


Fig. 1. Deep neural network structure.

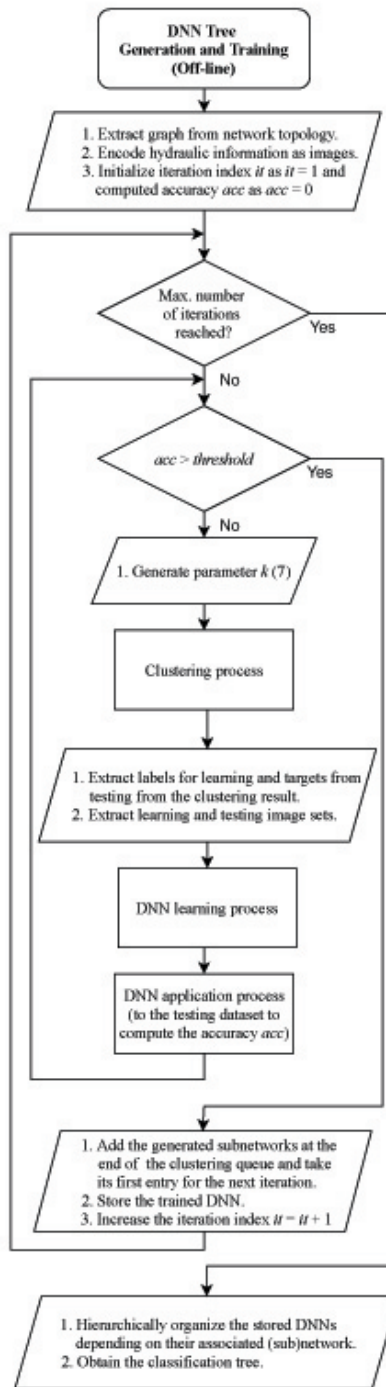


Fig. 2. Flow chart of the methodology steps for the learning (off-line) stage.

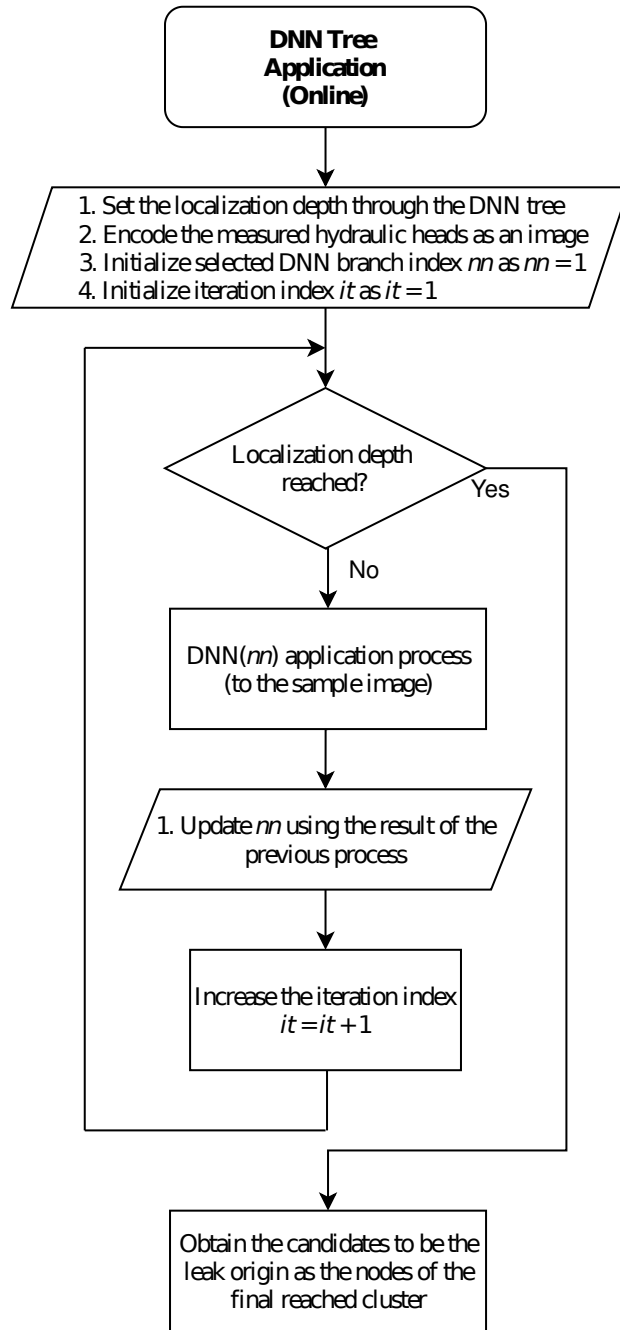


Fig. 3. Flow chart of the methodology steps for the application (online) stage.

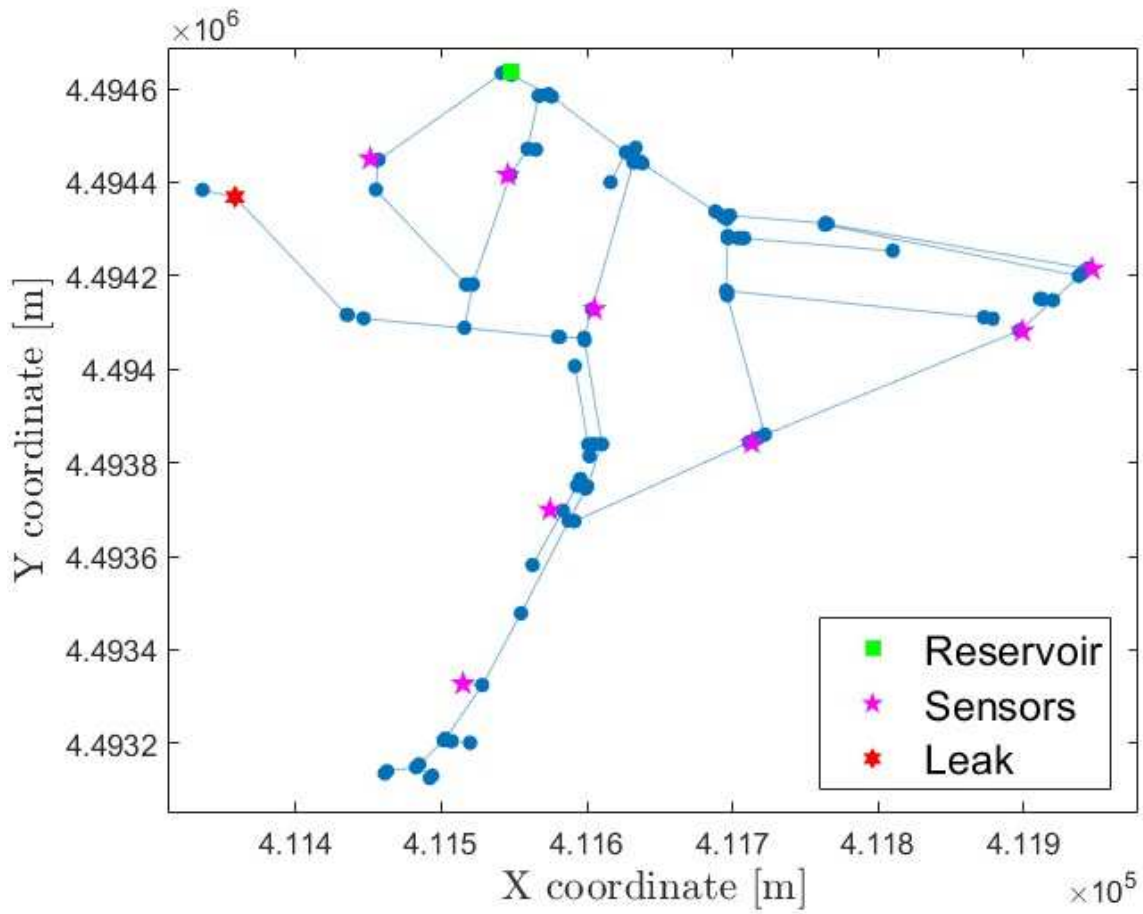


Fig. 4. Schematic representation of E-Town.

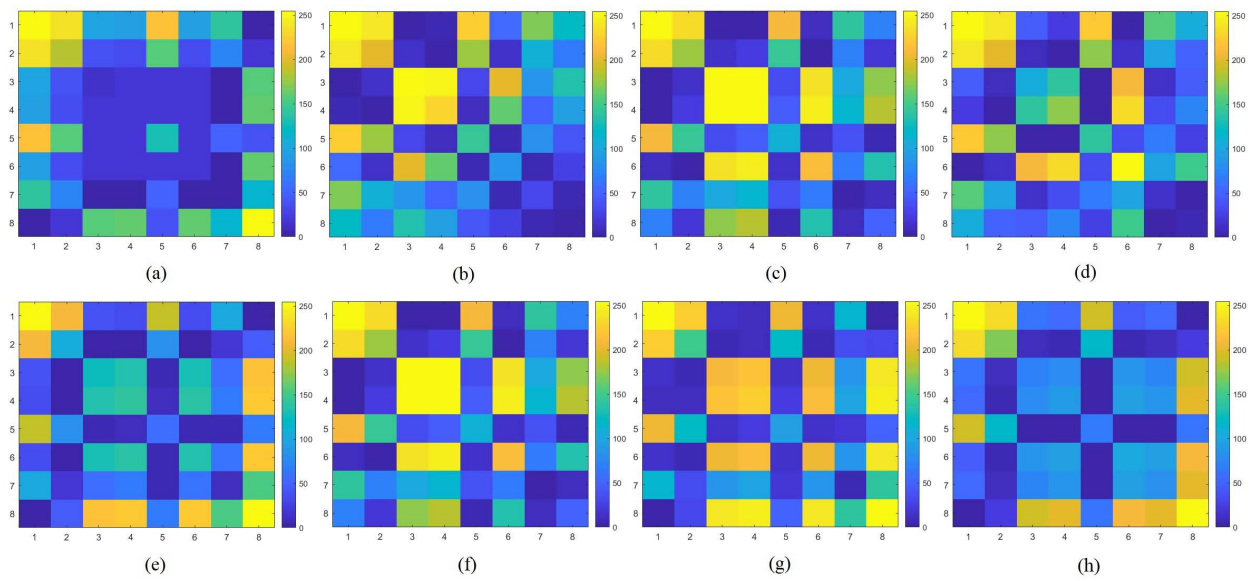


Fig. 5. A comparison among the GAF images associated to eight different leak events is presented. In appearing order: (a) Node 4, (b) Node 29, (c) Node 39, (d) Node 41, (e) Node 43, (f) Node 58, (g) Node 85 and (h) Node 94.

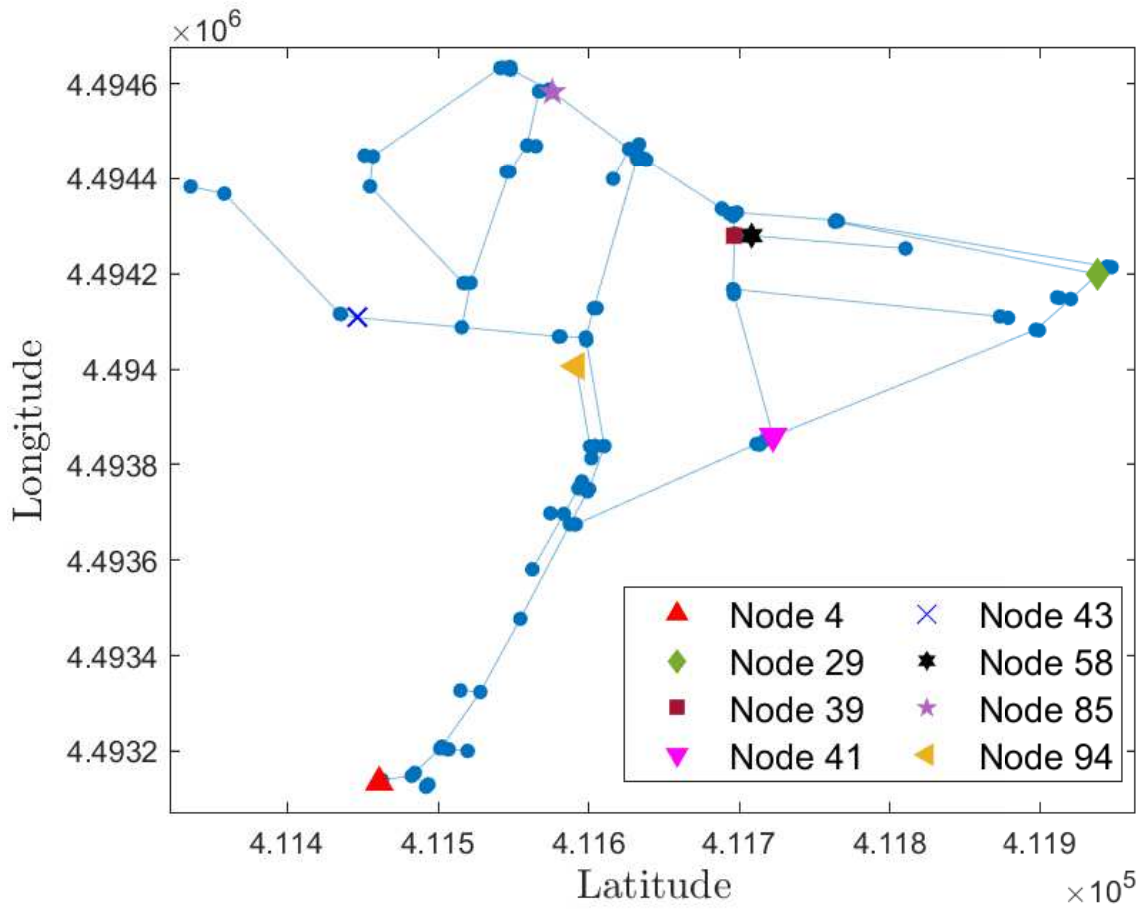


Fig. 6. Location of the considered nodes for the GAF demonstration.

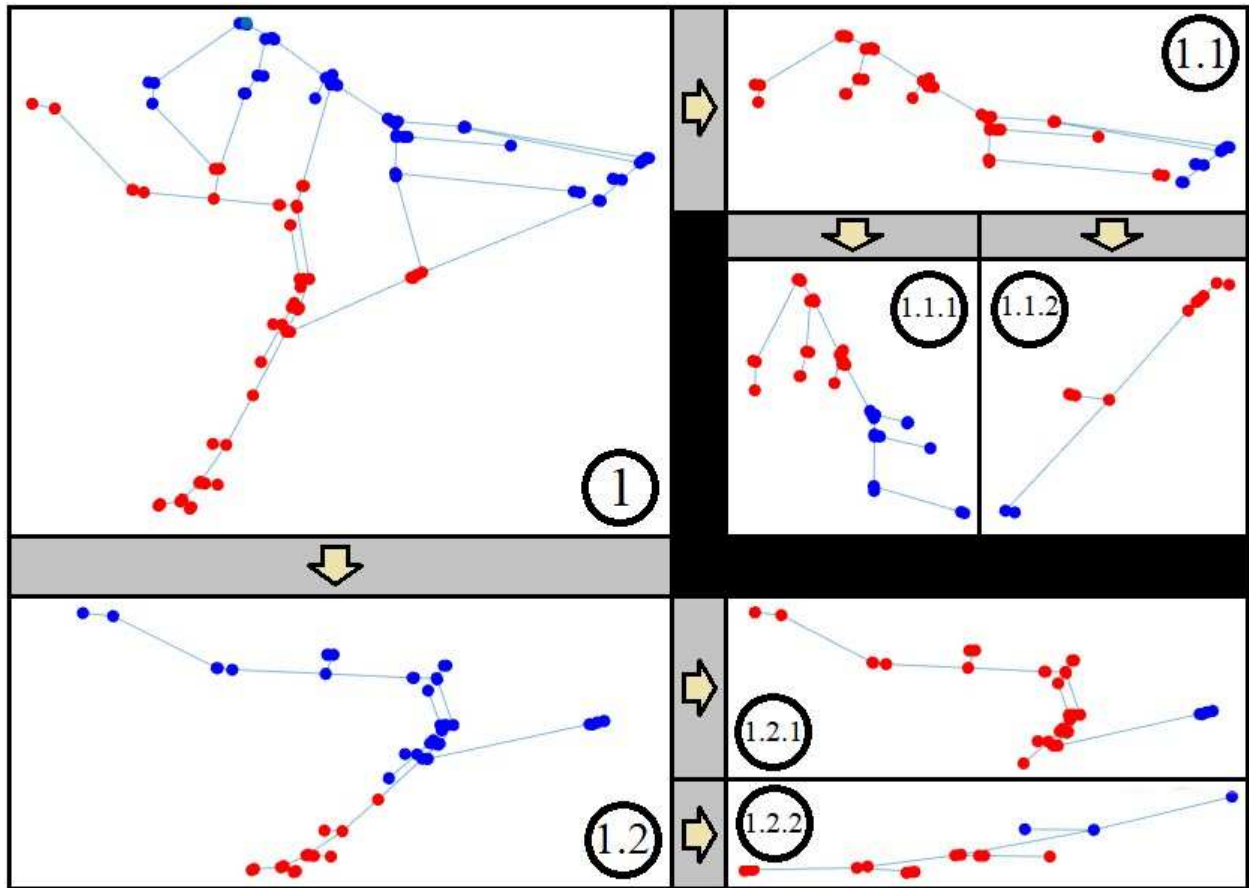


Fig. 7. Clustering results for E-Town until 8 clusters are achieved.

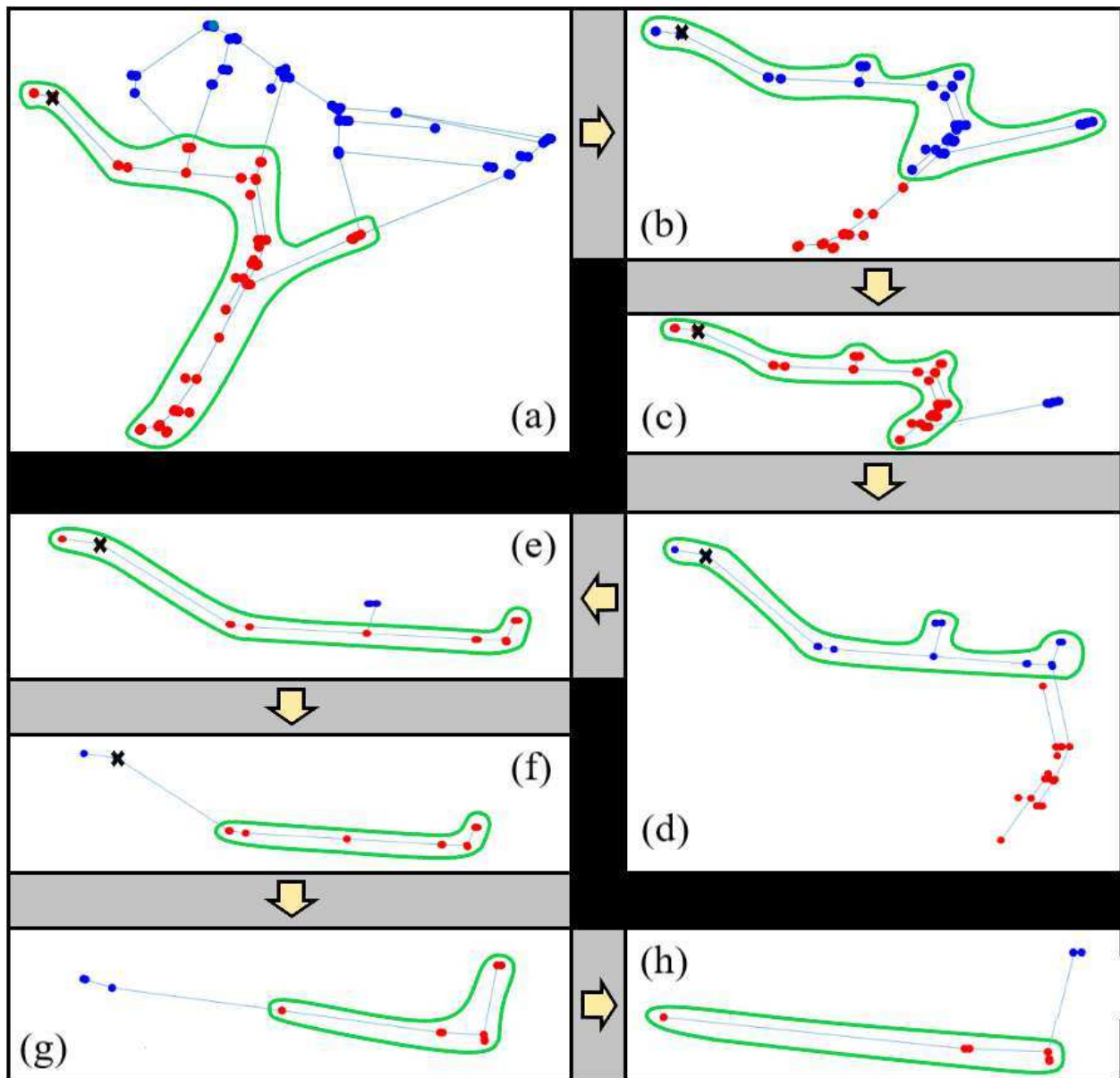


Fig. 8. Graphical summary of the localization process performance: (a) Complete network, (b) Subnetwork of the cluster selected from (a), (c) Subnetwork of the cluster selected form (b), (d) Subnetwork of the cluster selected form (c), (e) Subnetwork of the cluster selected form (d), (f) Subnetwork of the cluster selected form (e), (g) Subnetwork of the cluster selected form (f), (h) Subnetwork of the cluster selected form (g).

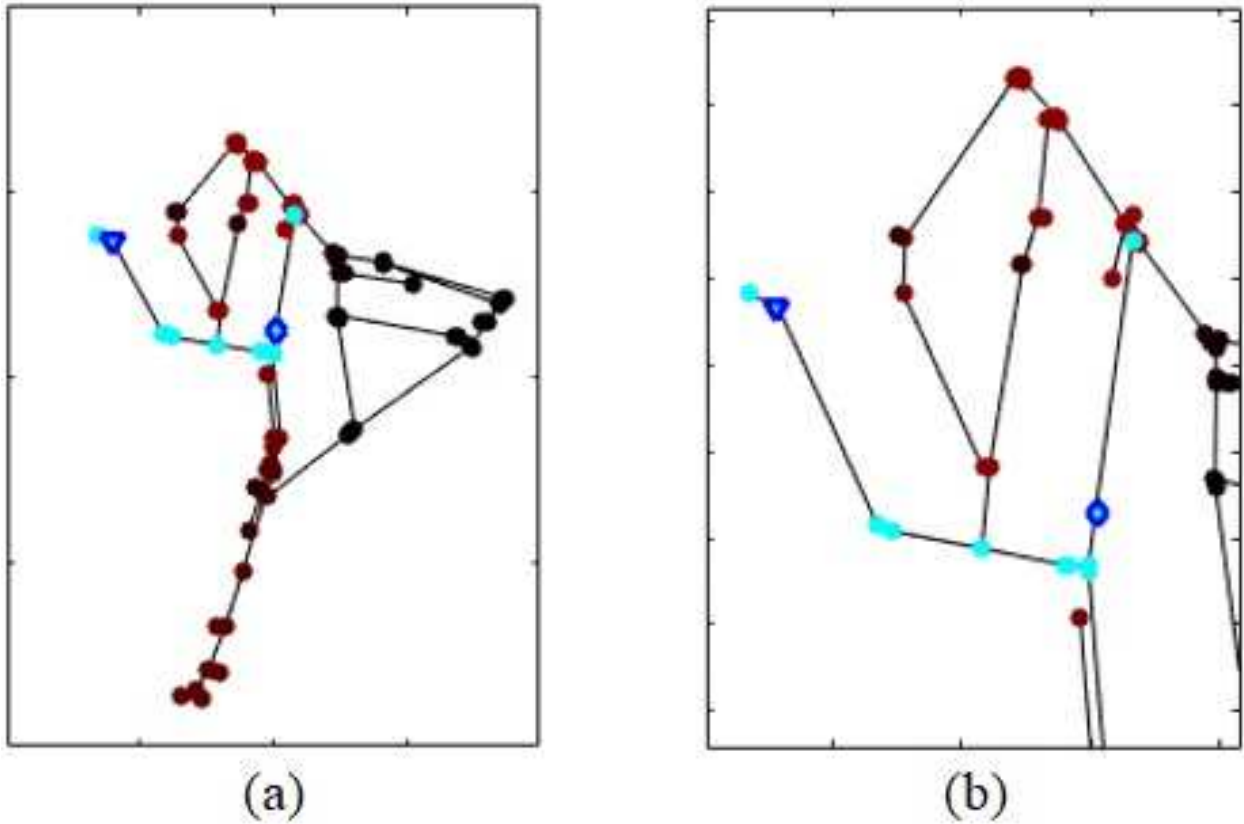


Fig. 9. Result of the application of a model-based approach to the leak localization of the real leak. (a) Correlations map - the bluer the node, the higher the correlation, and hence, the higher the probability of the node to be the origin of the leak. (b) Zoom of the most probable leak area.